Feasibility study of the photofission technique for characterization of 220-L concrete-lined nuclear waste drums at 7 or 9 MeV energies

Iaroslav Meleshenkovskii, Adrien Sari, Aly Elayeb, Roberto de Stefano

Feasibility study of the photofission technique for radiological characterization of 220-L concrete-lined nuclear waste drums using 7 or 9 MeV linacs

I. Meleshenkovskii[1*], A. Elayeb[1], R. De Stefano[1], A. Sari[1]

[1]Université Paris-Saclay, CEA, List, F-91120 Palaiseau, France

*Corresponding Author: Iaroslav Meleshenkovskii, iaroslav.meleshenkovskii@cea.fr

Abstract

Photofission is a promising technique for the radiological characterization of nuclear waste packages with dense and voluminous matrices. The goal of this paper is two-fold. First, we assess the performance of the photofission technique for the radiological characterization of a 220-L nuclear waste mock-up drum with a concrete liner and different uranium or plutonium samples and segmented hotspot detection using a 9 MeV linear electron accelerator (linac). Second, we build an MCNP6 numerical model of the measurement setup and validate it against the experimental data. Furthermore, using the validated MCNP6 numerical model at 9 MeV we assess the performance of the photofission technique at 7 MeV and with virtual cases, representing different homogeneous matrix materials that fill the entire volume of the mock-up drum. Results of this study indicate that the minimal detectable masses of depleted uranium and 94% ^{239}Pu samples obtained with a linac operated at 9 MeV and 100 Hz during 10 min are 0.539 and 0.336 grams respectively. The sensitivity for hotspot detection indicated a 6-times difference in the counting statistics in both scanning directions between the extremes and center position. The photofission rate with a linac operated at 7 MeV is poorer than that at 9 MeV by 15-times for all studied characterization cases. However, the characterization performance at 7 MeV could still be sufficient for actinide mass determination in concrete, plastic and metallic waste matrices, which fill the entire volume of a 220-L drum.

Keywords

Photofission; Delayed neutrons; Linear electron accelerator (linac); Nuclear waste package; Concrete matrix; Radiological characterization

1. Introduction

Nuclear waste package characterization is an important and challenging activity, which among others is accomplished via means of non-destructive assay. The challenges arise from the specific characteristics of such waste packages, which can be categorized on radiological, physico-chemical properties of the matrix material and type of the containment used for it. Thus, radiological properties of waste packages are determined by the presence of plutonium, uranium, fission products and minor actinides. The physico-chemical properties of the matrix material present in the waste package are determined by the type of waste matrix and its homogeneity. The containment characteristics can be represented by the size of the waste package and presence of concrete.

A combination of the aforementioned properties of waste packages determines a challenging nature of interactions of the radiation emitted by the assaying materials of interest (plutonium and uranium) and influences the detection accuracy and related uncertainties. Active non-destructive assay techniques, among others are used for characterization tasks of nuclear waste packages. The importance of the fissile material content quantitative characterization in nuclear waste and D&D operations is reflected in the EU Horizon 2020 MICADO project which aims

at application and assessment of various active non-destructive assay techniques for nuclear waste packages analysis [1]. Photofission-based active non-destructive assay was proposed as a promising technique to tackle the associated challenges and for waste packages containing concrete.

Photofission requires a linear electron accelerator (linac) as a source of interrogating *Bremsstrahlung* photons. Such linac systems can be operated at various energies and frequencies. Previous research in the domain of photofission application to waste packages characterization includes works of [2-10]. However, there have yet been no reference results reported for the radiological characterization of 220-L nuclear waste drums with different matrices by photofission using linacs operated at 7 and 9 MeV endpoint energies. In this paper, we aim to fulfil this gap by assessing the performance of the photofission technique experimentally at the SAPHIR platform (CEA Paris-Saclay) and by Monte Carlo simulations in the MCNP6 code.

Experimental results at 9 MeV are obtained using a 220-L concrete-lined mock-up drum with either depleted uranium or 94% ^{239}Pu samples. Counting of delayed neutrons from photofission is performed in the interpulse mode using ^{3}He counters, which are deployed as reference detectors. Hotspot detection is performed by segmented horizontal and vertical scanning of the nuclear waste drum in the ± 30 cm range relatively to the center of the sample. An MCNP6 simulation model of the measurement setup is validated relatively to the experimental results and is used to assess the performance of the photofission technique on virtual cases with different configurations of the matrices and at 7 MeV endpoint energy, which is not far from the photofission energy threshold for most actinides [10]. Detection efficiencies, effects of matrix density and hydrogen content in the 220-L waste package are also characterized at 7 and 9 MeV endpoint energies.

Evaluation of the photofission technique performance using a 7 MeV linac represents a strong interest for future applications aiming at designing a compact mobile system dedicated to *in-situ* measurements. This interest is driven by a lower dose-burden impact during their operation and hence less complicated shielding configuration as well as compact design of such systems making them feasible for mobile platforms.

2. Materials and methods

2.1. Experimental setup

Reference measurements were conducted at the SAPHIR platform at CEA Paris-Saclay. A schematic layout of the main parts of the measurement system used in the present work is shown in Fig. (1).

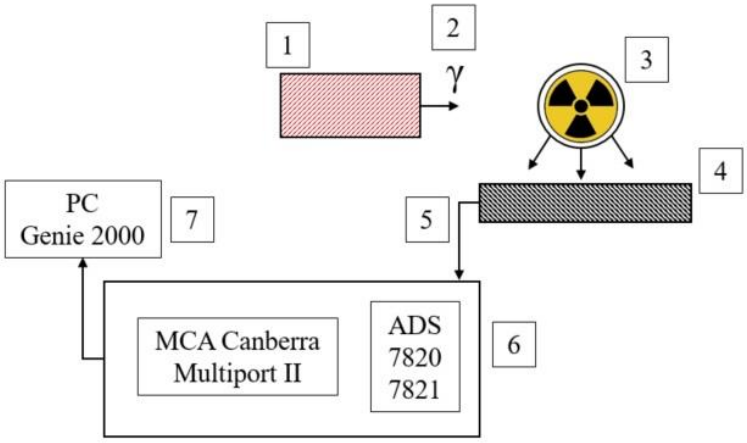

Fig. 1. Schematic layout of the setup.

In Fig. (1) the following major components of the measurement instrumentation are shown: *1* is the Linatron-M9 linac (Varex Imaging); *2* is the collimated beam of *Bremsstrahlung* photons emitted in the direction of the sample; *3* is the sample and/or mock-up drum; *4* represents the detection block; *5* are the connecting cables between the detectors and read-out electronics; *6* is the read-out electronics and high-voltage power supply; *7* is the operating personal computer (PC) with installed Genie 2000 data acquisition software.

The detection block was comprised of five ^{3}He filled one-meter long tubes (150NH100) at 4 bars pressure in a high density polyethylene matrix (ρ=0.965 g/cm^{3}) and cadmium casing of 1 mm thickness. The detectors were put aside of the photon beam trajectory to reduce the blinding effect of the detectors and placed at a distance of 1 m from the nuclear samples position. The detectors were connected to the read-out electronics via Draka Fileca F1209-8 cables. The read-out electronics was comprised of Canberra ADS 7820, MCA Multiport II and high-voltage power supply 7821 providing the detectors with 1500 V bias voltage. A general view of the experimental setup is shown in Fig. (2).

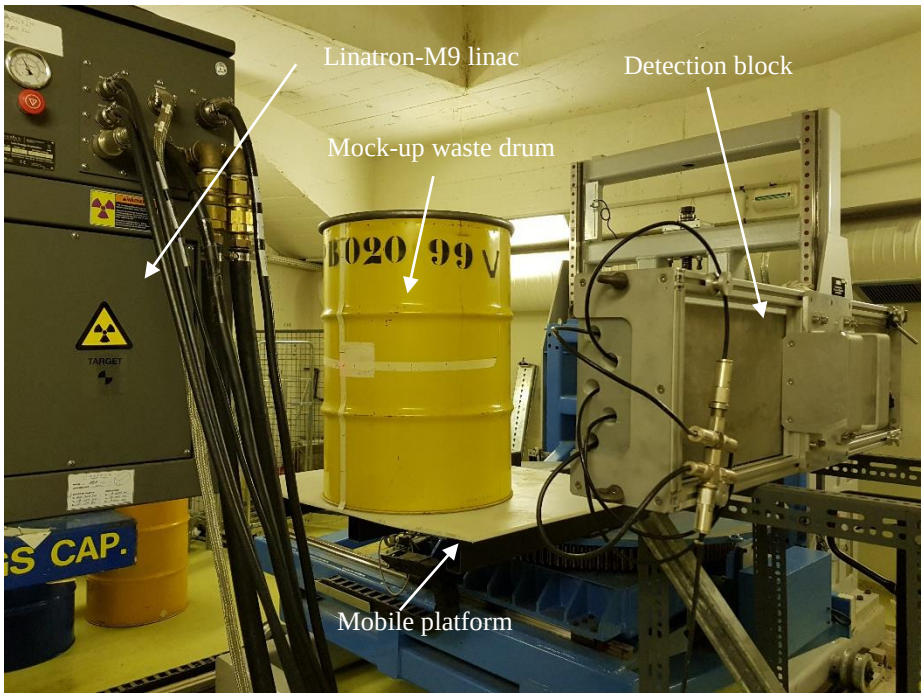

Fig. 2. Overview of the experimental setup at the SAPHIR platform (CEA Paris-Saclay).

A beam of electrons is projected onto a tungsten target, producing the *Bremsstrahlung* photons. The electron peak current is 100 mA and the electron pulse duration is 2.5 μs. The energy distribution and other qualitative and quantitative flux characteristics of the tested system are described in detail in [8, 10]. The linac can be operated at various frequencies. However, in this study we used 100 Hz as operating frequency for all tests carried out. A schematic chronogram of the linac pulsed operational mode is presented in Fig. (3).

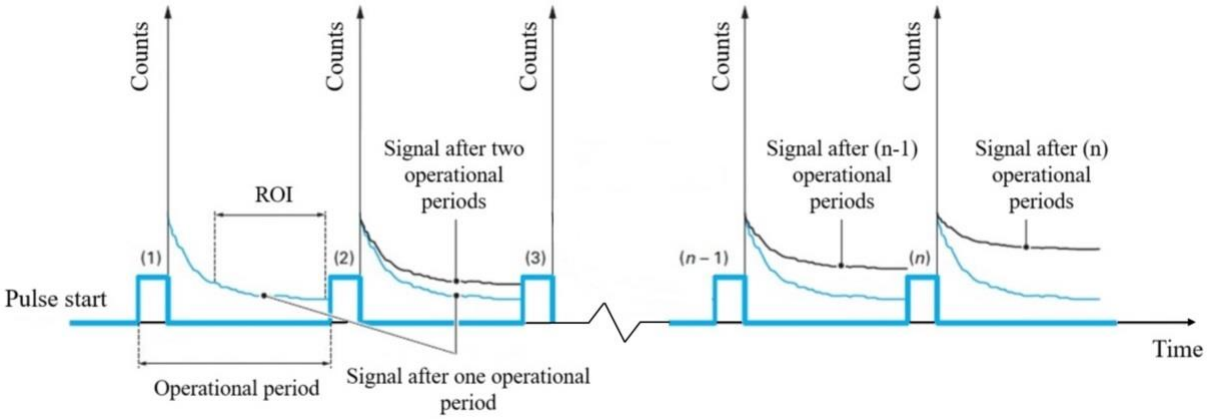

Fig. 3. Schematic chronogram of the interpulse counting mode of delayed neutrons from photofission.

The produced *Bremsstrahlung* photons follow the collimator channel with a cone-shaped opening directing the beam at the mock-up drum. Besides the *Bremsstrahlung* photons, parasitic photoneutrons are produced as in the target as well as in the collimator channel materials due to the low (γ, n) threshold reaction of tungsten (around 7 MeV). Assessment of the photoneutron production and ways of its minimization are described in previous work [10]. However, in the results presented in this work we did not use any specific measures for parasitic neutron suppression and kept the original configuration at the SAPHIR platform (CEA Paris-Saclay). The mock-up drum is positioned on a mobile platform allowing to change its vertical and horizontal coordinates. In this study, the position of the detection block was fixed in all our tests and was 1 m from the center of the drum. The mock-up drum was positioned at 1 m from the target of the linac.

2.2. Mock-up drums and samples

The mock-up drum used for tests in this study has a 6.5 cm thick concrete liner, as shown in Fig. (4). Samples were positioned in the center of the drum at half of its height.

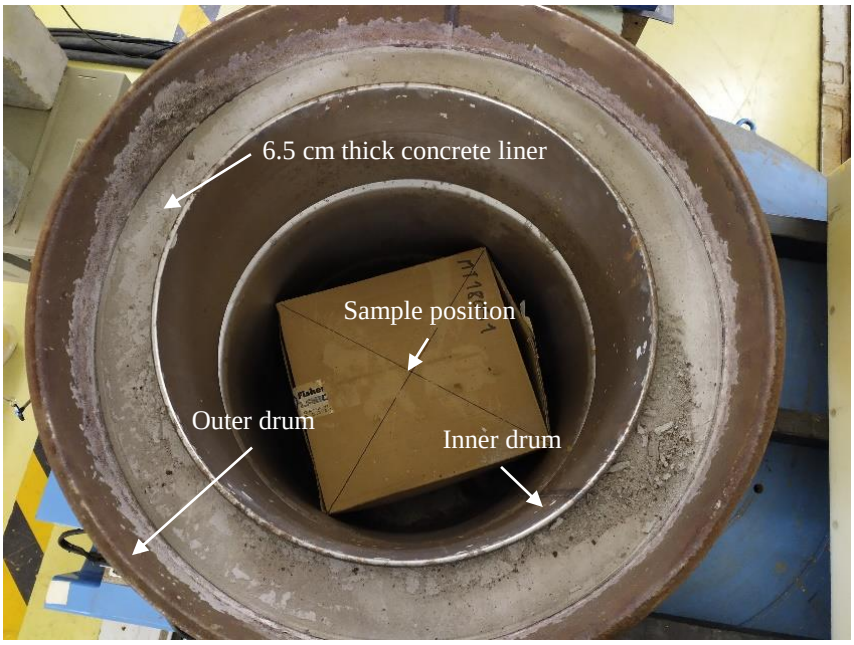

Fig. 4. Mock-up drum with a concrete liner.

The dimensions of the drum are: 80 cm of height, 57.5 cm of diameter of the outer drum and 1 mm wall thickness. The diameter of the inner drum is 44 cm. The outer drum material is ordinary carbon steel (ρ=7.85 g/cm^3), the inner drum material is stainless steel (ρ=7.9 g/cm^3). The concrete liner (ρ=2.4 g/cm^3) elemental composition is displayed in Table (1). The total volume of the tested mock-up drum is 220 L.

Table 1. Concrete composition.

Element	**Weight fraction, %**
H	0.75
C	0.1
O	52.9
Na	1.6
Mg	0.2
Si	33.7
K	1.3
Ca	7.8
Fe	1.4

The nuclear materials used in this study were comprised of three AmLi sources, metallic depleted uranium samples (0.3 % enrichment) and a plutonium sample with 94% of ^{239}Pu isotope (PIDIE sample [11, 12]). The characteristics of AmLi sources at the date of the experiment are presented in Table (2).

Table 2. AmLi source characteristics.

Type of AmLi source	Data on 19.04.2021	
	Activity, GBq	Neutron emission, n/s
AmLi n° 1327	38.07	41157
AmLi n° 1328	33.14	35827
AmLi n° 1329	39.08	42252

2.3. Monte Carlo simulation model

To allow for assessment of the virtual cases with parameters (*e.g.* matrix composition, electron energy) that extend the experimentally measured cases a Monte Carlo simulation model was developed. In this study, the MCNP6 Monte Carlo simulation code was used [13]. The model of the experimental setup consisted of a Linatron-M9 linac (Varex Imaging), a 220-L mock-up drum and a detection block with five one meter-long ^{3}He counters (150NH100). Fig. (5) shows a 3D view of the simulation model. The surrounding environment was also included in the model and was comprised of air, concrete walls, floor and ceiling of the facility.

The main parts of the linac include a cylindrical collimator body, target material, beam stop plate positioned after the target and cone-shape collimator. Simulation statistics for all studied cases was chosen so that the resulting tallied uncertainties on the photofission rates and detection efficiency are around 1 %.

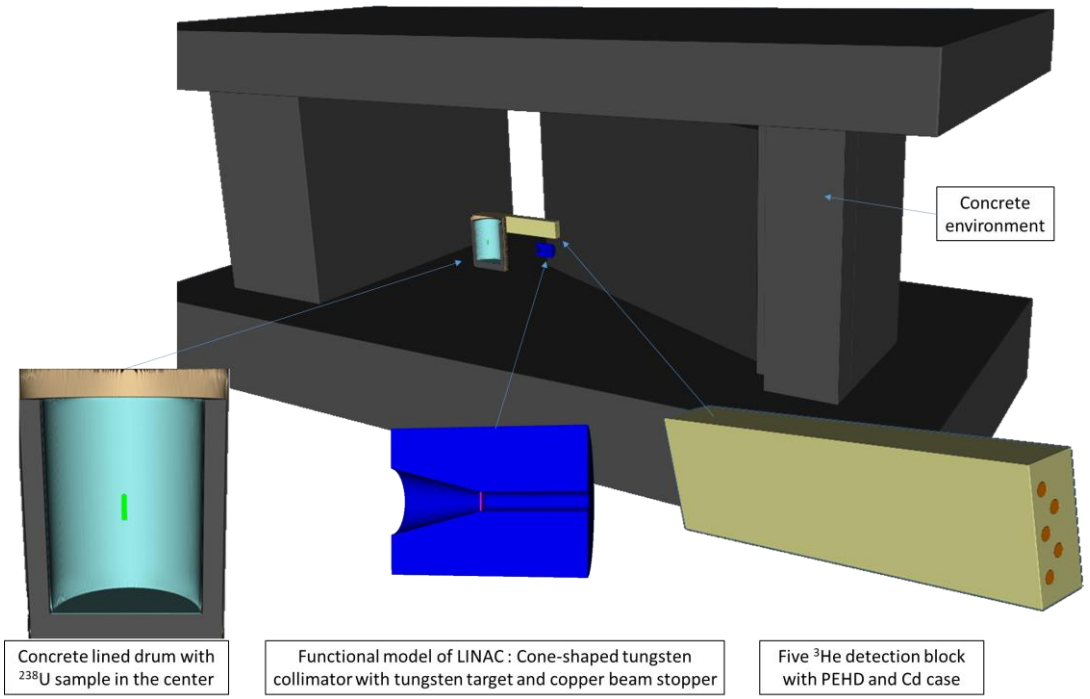

Fig. 5. 3D view of the MCNP6 simulation model.

Characterization of the photon and photoneutron fluxes for the Linatron-M9 linac is provided in two previous studies [8, 10].

2.4. Detection methodology

The choice of the detection methodology depends on different factors and specific requirements set for the assay system. Among such influencing factors are the detection sensitivity, timeliness of measurements as well as the cost.

The high-energy photons (> 6 MeV) have the power to penetrate dense matrix materials and induce the fission reaction of heavy nuclei. By knowing the characteristics of the interrogating high-energy photon beam exceeding 6 MeV (energy, intensity, frequency, direction, *etc.*), the measurement of various fission signatures allows qualitative and quantitative characterization of actinides present in the analyzed package.

With photofission assay technique, different signatures can be used. However, direct detection of prompt gamma-rays is not possible due to the gamma flash delivered by the linac and resulting blinding time of the detectors. Detection of prompt neutrons can be realized via advanced activation techniques using response converters [14].

Detection of delayed signatures can be done for both neutrons and gamma-rays. The detection methodology can be based on interpretation of the total neutron and/or photon (above 3 MeV) count rate or delayed gamma-ray spectrometry. The former represents somewhat a traditional methodology, benefiting from a straightforward application of the traditional ^{3}He detectors (for delayed neutrons) and scintillation detectors (for high-energy delayed gamma-rays). Delayed gamma-ray spectrometry represents an advanced detection methodology in which the delayed gamma-ray spectrum acquired with high-resolution HPGe detectors is used to infer the information about the actinides isotopic composition [15-19].

Photofission allows using of the two different counting modes – the so-called "interpulse" and "post-irradiation" modes (or sometimes so-called "macropulse"). In the "interpulse" mode, counting is done in-between of the linac pulses. In the "macropulse" or "post-irradiation" mode, delayed neutrons and/or gamma-rays are measured after the irradiation. The delayed neutrons and gamma-rays are emitted by the precursor nuclei of fission products after photofission (representing six delayed neutron and five delayed gamma-ray groups).

In the present work, detection of delayed neutrons from photofission in the "interpulse" mode was used for all experiments with ^{3}He counters as reference detectors.

3. Results and discussion

3.1. Measurement protocol

The measured signal from a 241 g depleted uranium sample and active background is presented in Fig. (6). The acquisition time was 10 min for each of the cases. Integration of the signal was done for 60000 irradiation cycles as the linac was operated at 100 Hz. The electron peak current at the target was 100 mA and the pulse duration was 2.5 μs.

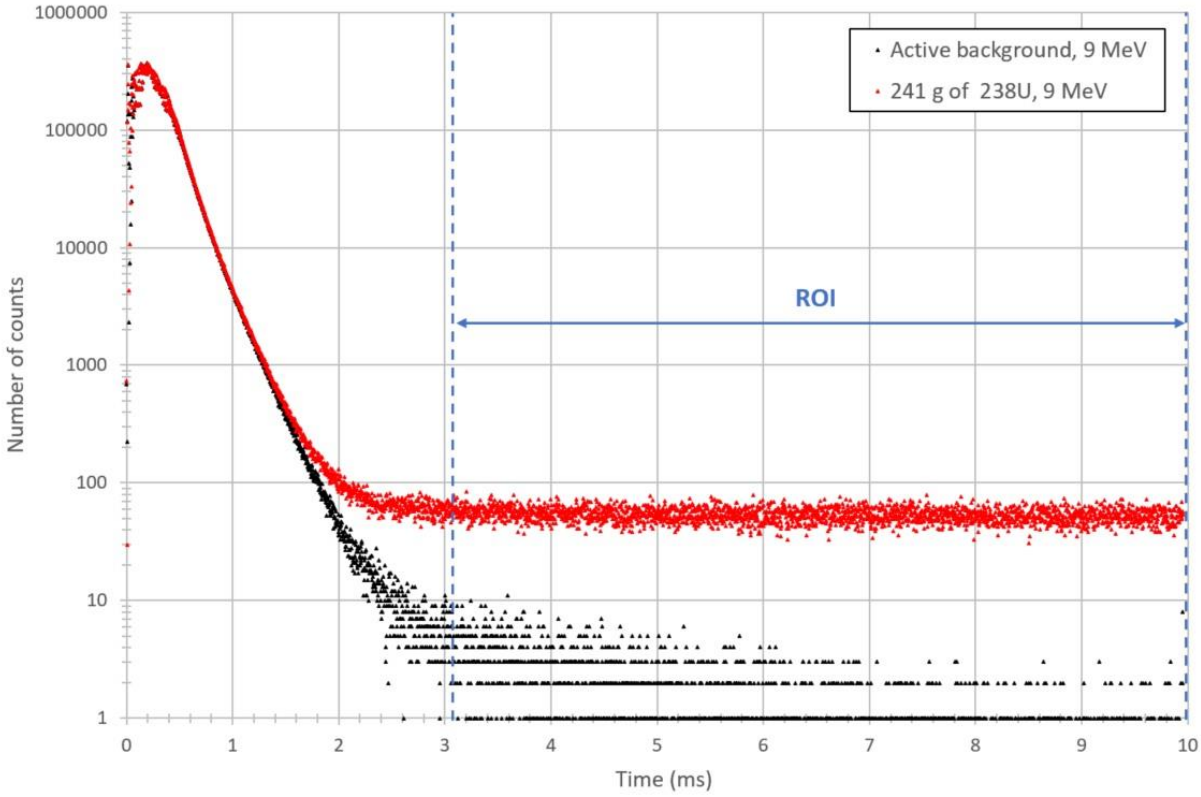

Fig. 6. Measured response from depleted uranium sample and active background at 9 MeV integrated for the 60000 irradiation cycles.

From Fig. (6) it can be noticed that up to 3 ms there is a strong impact of the gamma flash induced by the linac and of photoneutrons due to (γ, n) reactions in the target and collimator materials. The gamma flash leads to a significant blinding time of the detectors. Presence of the parasitic signal is clearly visible in the case of active background counting, with no sample in the vicinity of the beam. For this reason, the delayed neutron counting window in our experiments was selected to start from 3 ms up to 10 ms.

3.2. Absolute detection efficiency

The absolute detection efficiency of delayed neutrons from photofission measured with one detection block composed of five ^{3}He tubes was determined in two major configurations – with and without the concrete lined mock-up drum. These calculations were done using a set of three AmLi sources (described respectively by the following numbers: 1327, 1328 and 1329). The results of the detection efficiency determined from experimental measurements (at the SAPHIR platform, CEA Paris-Saclay) or by Monte Carlo simulation with the MCNP6 code are summarized in Table (3).

Table 3. Results of the absolute detection efficiency calculations for delayed neutrons from photofission measured with one detection block.

Neutron source	**Configuration**		
	Experimental results		**MCNP6 results**
	Absolute detection efficiency without the mock-up drum, %	**Absolute detection efficiency with the source inside the mock-up drum, %**	**Absolute detection efficiency with the source inside the mock-up drum, %**
AmLi n° 1327	0.264	0.258	0.265
AmLi n° 1328	0.246	0.240	
AmLi n° 1329	0.269	0.267	
Mean value	*0.260*	*0.255*	

Our experimental results indicate that there is a loss of 2% in the absolute detection efficiency due to the concrete lined (6.5 cm-thick) mock-up drum. The simulated absolute detection efficiency was 0.265 %, what is within 4 % of accuracy relatively to the mean experimental value achieved. Results confirm that concrete thermalizes neutrons, except that only 7 % of the neutrons either get absorbed or thermalized below the cadmium energy cutoff of the detection block. However, this thermalization of neutrons by the concrete liner also contributes to a better detection in the ^{3}He detectors, which partly counterbalances the 7% loss in the concrete.

Another important aspect is related to the portion of photoneutrons that is present in the interrogation flux causing neutron-induced fissions. Since in this study we did not use any specific measures for parasitic neutron suppression, keeping the original configuration at the SAPHIR platform (CEA Paris-Saclay), an estimation of the relative portion of photon- and neutron-induced fissions in the sample at 7 and 9 MeV was conducted using Monte Carlo simulations. The assessment was conducted for a reference 220-L mock-up drum with a depleted uranium sample positioned in its center like the beam projection. The results are summarized in Table (4).

Table 4. Photon and neutron induced fissions at 7 and 9 MeV.

Energy, MeV	**Fission mode**	
	Photon-induced fission, s^{-1}	**Neutron-induced fission, s^{-1}**
7	1.73E+06 (δ=1.27 %)	6.78E+04 (δ=4.23 %)
9	2.38E+07 (δ=0.89 %)	1.04E+06 (δ=2.85 %)

Results from Table (4) indicate that the relative portion of fissions caused by photoneutrons at 7 and 9 MeV energies is 3.9 % and 4.4 % respectively. A *yz* view of the neutron flux cartography within the drum is shown in Fig. (7).

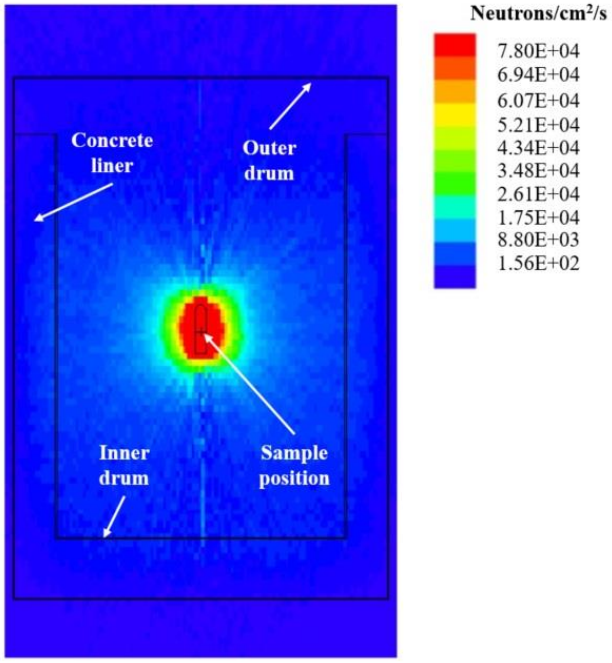

Fig. 7. YZ view of the neutron flux cartography within the drum.

3.4. Nuclear material mass sensitivity

To determine the fissile mass detection sensitivity curve we used a measurement configuration without mock-up drums. Thus, samples of 241 grams of depleted uranium (0.3 % enrichment) in metallic form were put together and centered in the beam *y*-axis. Determination of the fissile mass sensitivity curve for the case with four samples was conducted for two specific configurations, as shown in Fig. (8). The studied cases are denoted *a* and *b*, representing "favorable" and "unfavorable configurations". The individual photofission rates (s^{-1}) for each of the samples in all studied measurement configurations are also provided in Fig. (8).

As the Linatron-M9 linac can also be operated at 6 MeV, which is more or less the energy threshold of the photofission reaction for most actinides, this electron energy was also tested in addition to 9 MeV. Determination of the sensitivity curve at the two different electron energies was driven by the interest to study the behavior of close to the photofission threshold and sufficiently exceeding that boundary incident energies. The resulting detection sensitivity curves determined at 6 and 9 MeV are displayed in Figs. (9)-(10) respectively. The standard uncertainty bars are within the size of the corresponding data points. The observed difference expressed in a curve drop at the point of 964 grams is due to the different attenuation behavior of the incident photon beam.

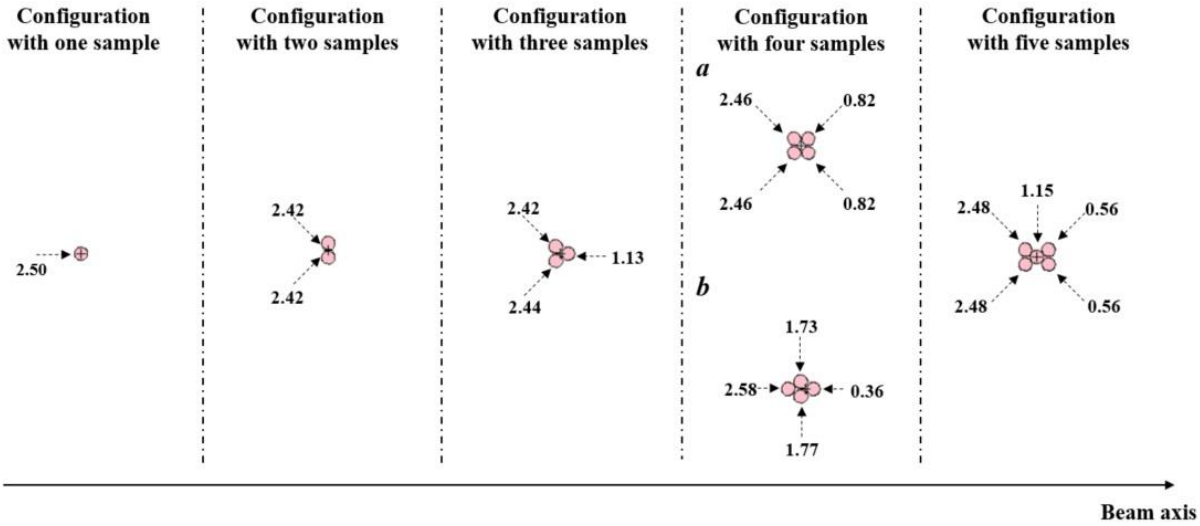

Fig. 8. View according to the beam axis of the studied measurement configurations with depleted uranium samples put together at 9 MeV (sample size is not to scale; all photofission rate exponents are 10^7).

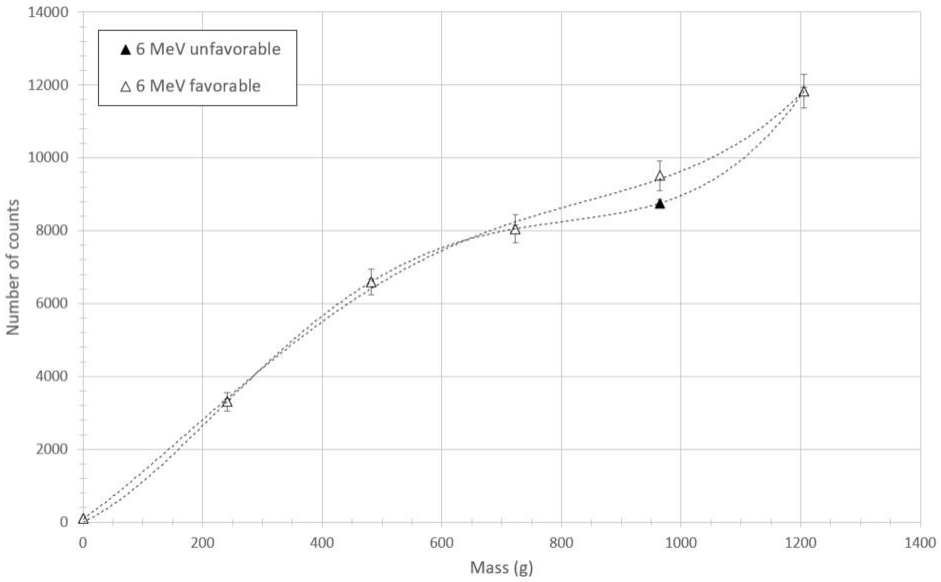

Fig. 9. Delayed neutron counts as a function of the depleted uranium mass, obtained at 6 MeV.

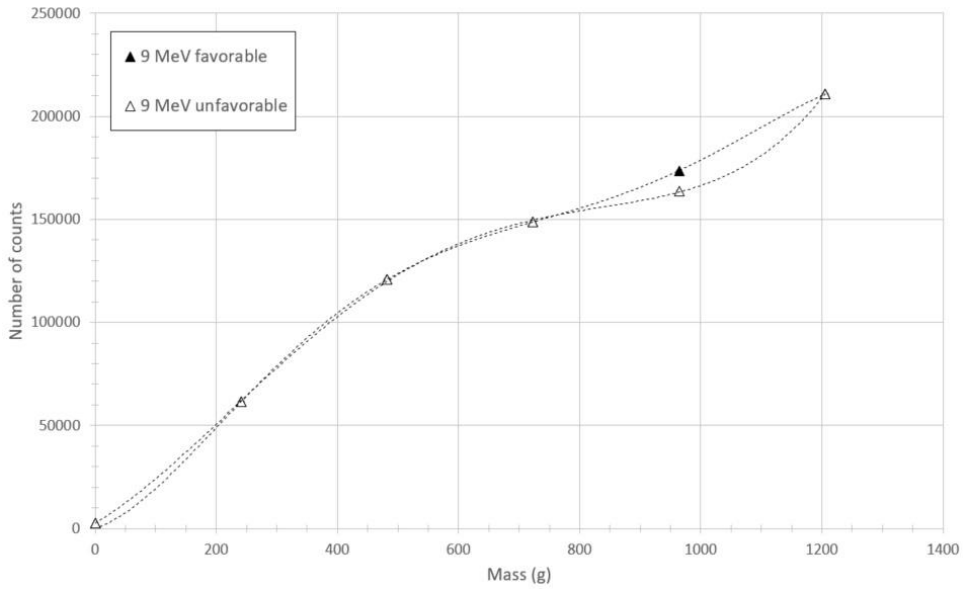

Fig. 10. Delayed neutron counts as a function of the depleted uranium mass, obtained at 9 MeV.

3.4. Vertical and horizontal scanning of the drum

The idea behind such an assessment is to gain knowledge on the possibility of scanning the drum according to the height and the sides to localize some potential hot spots. Horizontal and vertical scanning of the drum enables to localize potential hot spots that can further be inspected more thoroughly in a second step. To determine the impact of the mock-up drum geometrical positioning on the counting statistics the sample was fixed at the center of the drum, while the drum position was shifted along the horizontal (y) and vertical (z) beam axes, as shown in Fig. (11). The horizontal scanning is performed with (z) = 0 (center of the drum). The position shifting increment was 5 cm in y-axis and 10 cm in the z-axis, with a more frequent scaling near the center of the drum. The drum is moved thanks to a mobile platform. The beam location uncertainty is of the order of ± 4 mm.

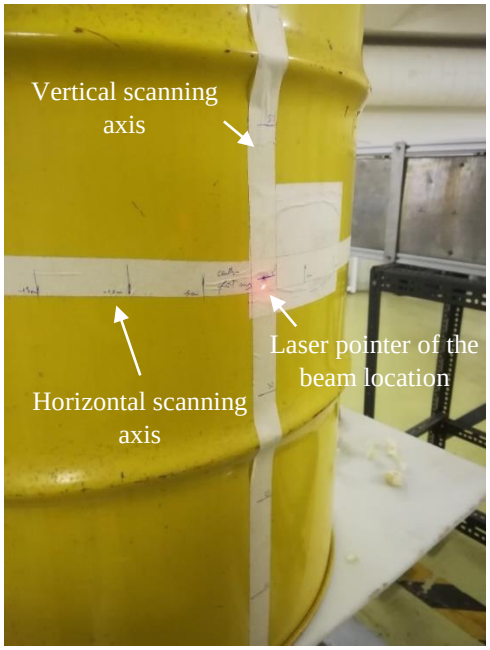

Fig. 11. Mock-up drum positioning geometry.

Counting of the delayed neutrons from photofission was performed for multiple measurements with the drum set in a given position. The horizontal and vertical scanning results are respectively displayed in Figs. (12)-(13). The standard uncertainty bars are within the size of the corresponding data points.

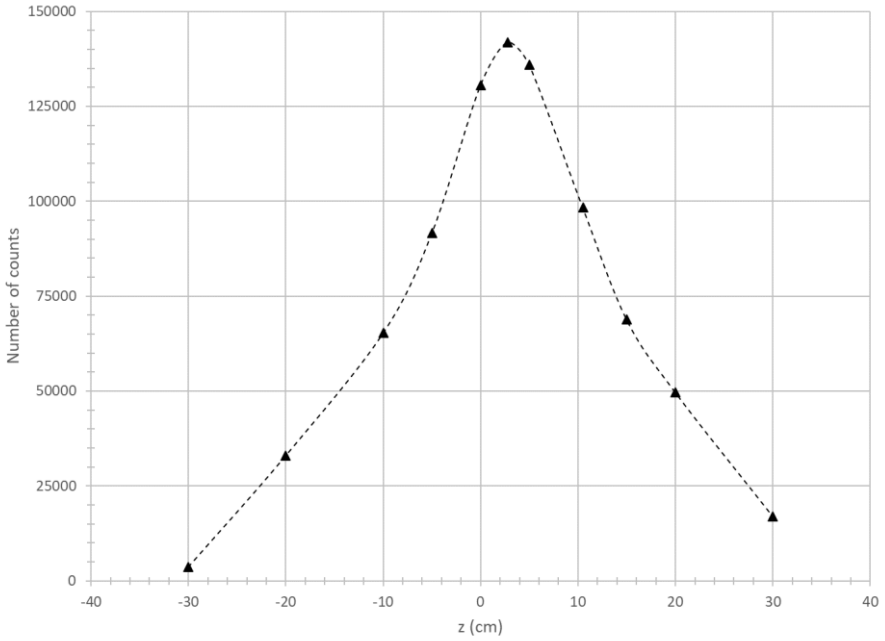

Fig. 12. Vertical scanning of the drum.

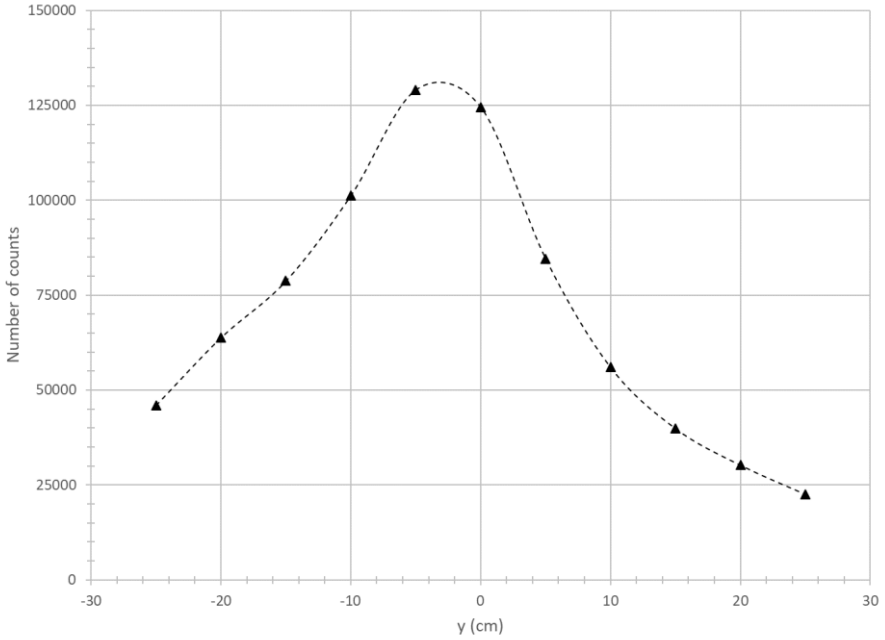

Fig. 13. Horizontal scanning of the drum.

Counting statistics indicated high sensitivity of the beam positioning (along horizontal *y* and vertical *z* axes) relatively to the center of the sample.

3.5. Detection limits

In active non-destructive measurements, the useful portion of the signal is superimposed on the background (BKG) continuum. The nature for this background radiation in photofission-based measurement techniques is due to photoneutron interactions, secondary reactions in the sample and surrounding materials. The knowledge of the background continuum level is important for measurements with low-mass fissile materials. To determine the detection limits for a non-detection and false alarm risk described by α and β factors equal to 2.5 %, we use a first approximation described by equation Eq. 1 [20]:

$$DL \approx 3.92 \times \sqrt{2 \times BKG} \qquad (1),$$

Where *DL* is the detection limit and *BKG* is the active background measured for the given configuration without the fissile material. Both *DL* and *BKG* are expressed in counts.

The detection limit is then divided by the measured signal per fissile material mass (denoted g^{-1}), which represents sensitivity coefficient. Calculations were done for a metallic uranium (241 grams) and a 94% ^{239}Pu samples at 9 MeV positioned inside the mock-up drum and are summarized in Table (5). The acquisition time was set at 10 min.

Table 5. Detection limits at 9 MeV.

Sample	**Active background, counts**	**Raw signal, counts**	**Net signal, counts**	**Detection limit, counts**	**Sensitivity coefficient, counts.g^{-1}**	**Detection limit, g**
Plutonium	2438	2784	346	273.72	814.1	0.336
Depleted uranium		124810	122372		507.8	0.539

The minimal detectable masses that can be determined with such a system operated at 9 MeV and 100 Hz are 0.336 grams for plutonium and 0.539 grams for uranium. The ^{239}Pu sensitivity is 1.6 times higher than that of ^{238}U, which is consistent with the ^{239}Pu/^{238}U photofission cross-section ratios.

3.6. Assessment and validation of the Monte-Carlo simulation model

The goal of this Monte Carlo simulation study was to assess and validate the numerical model representing the experimental measurement setup, described in Section 2. The numerical model was designed using the MCNP6 code and was comprised of the following components: linac, mock-up drum (with the concrete liner), the depleted uranium sample (0.3 % enrichment), the detection block with its five ^{3}He counters and the facility environment, which is comprised of the surrounding concrete walls, ceiling and floor. In the simulation model, the electron energy of the linac was fixed at 9 MeV. The position of the sample was kept in the center of the drum at half of its height.

The simulation routine was organized in four consecutive steps. In the first step, a simulation consisting of a detailed linac model, surrounding concrete background and a mock-up drum with depleted uranium sample was conducted. The output of this step was the knowledge on the photofission rate per incident electron. For this simulation, the F4:p tally was used in conjunction with FM4(-1 *m* 18), with *m* being the material number used to describe the ^{238}U

sample and 18 the MT reaction identifier for photofission inside the sample. In the second step, the photofission rate was converted to take into account the linac parameters, namely the 100 Hz operating frequency, 100 mA electron peak current and 2.5 µs pulse duration. This provided the output in photofission rate per second. The conversion factor expression is given by Eq. (2):

$$f(\nu) = \frac{I}{e} \times t_{irr} \times \nu = 1.56038E + 14 \qquad (2)$$

Where I is the electron peak current (100 mA), e is the elementary electron charge (1.602E-19 C), t_{irr} is the pulse duration (2.5 µs), ν is the linac operating frequency (100 Hz).

In the third step, the linac model was removed from the simulations. Instead, a detection block was added to the simulation model consisting of a mock-up drum and surrounding concrete background, and a delayed neutron emission spectrum sourced from ENDF/B-VII.0 database was set inside the depleted uranium sample, assuming its homogeneous distribution. At this step the detection efficiency was simulated using the F4:n tally in conjunction with FM4 (-1 *m* 103), with *m* being the material number used to describe the ^{3}He inside the detector and 103 the MT reaction identifier for the (n, p) reaction inside the detector. Finally, in the fourth step a conversion of the MCNP6 output of step three was conducted to obtain the number of counts in the detectors. For this step, the outputs of steps two and three were used along with the factor of electronic losses in the acquisition system.

In order to assess the behavior of the MCNP6 model, we simulated both horizontal and vertical scanning of the drums and compared the results relatively to the experimental data acquired at the SAPHIR platform. A 2D view of the measurement configuration used in this study is shown in Fig. (14). Simulated data are summarized in Tables (6)-(7) for vertical and horizontal coordinates respectively.

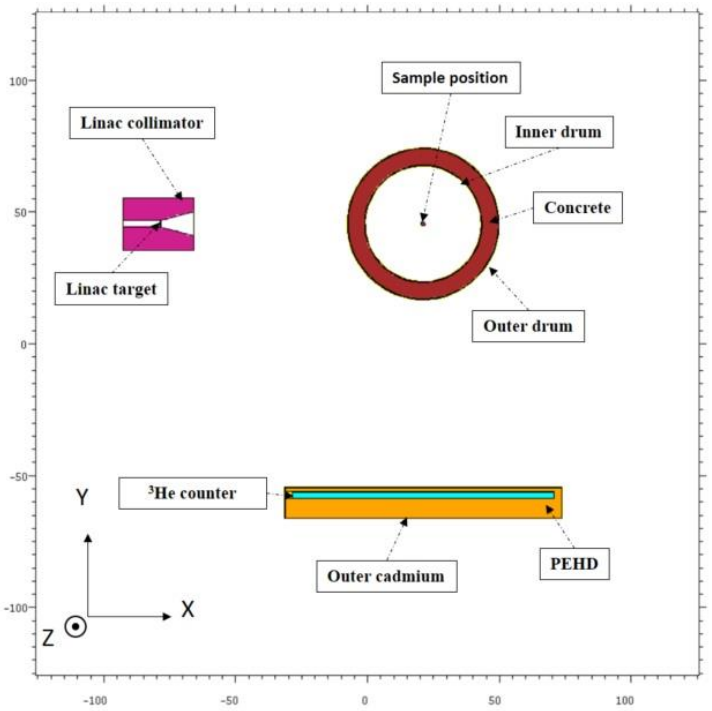

Fig. 14. 2D view of the measurement configuration model used in MCNP6 simulations.

Table 6. Simulated data at 9 MeV for vertical coordinate.

Position according to the z-axis	Photofission rate, fission/s	Detection efficiency, %
-30	4.58E+06	0.208
-20	7.92E+06	0.241
-10	1.51E+07	0.248
-5	2.06E+07	0.251
0	2.38E+07	0.250
2.75	2.32E+07	0.248
5	2.12E+07	0.248
10.5	1.56E+07	0.241
15	1.13E+07	0.235
20	8.28E+06	0.228
30	4.84E+06	0.217

Table 7. Simulated data at 9 MeV for horizontal coordinate.

Position according to the y-axis	Photofission rate, fission/s	Detection efficiency, %
-25	7.20E+06	0.388
-20	9.17E+06	0.354
-15	1.24E+07	0.326
-10	1.72E+07	0.297
-5	2.34E+07	0.272
0	2.38E+07	0.250
5	1.86E+07	0.232
10	1.34E+07	0.218
15	9.90E+06	0.198
20	7.42E+06	0.189
25	5.46E+06	0.175

Based on the simulated data presented in Tables (6)-(7) the corresponding counting rates were determined at each position. Figs. (15)-(16) compare the vertical and horizontal scanning of the drum obtained by MCNP6 simulation and experimentally at the SAPHIR platform.

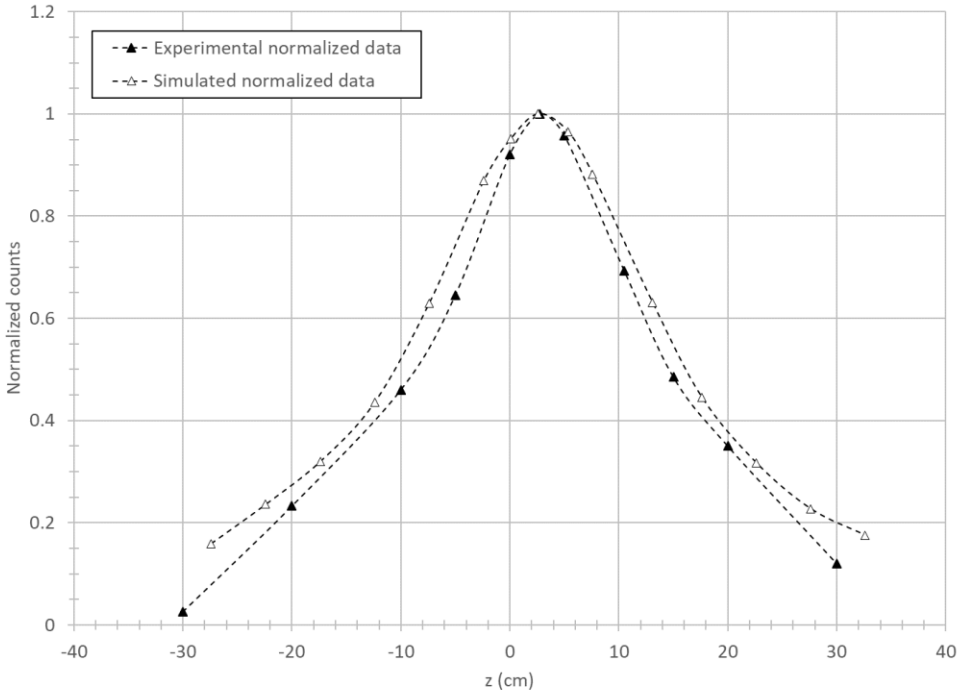

Figure 15. Comparison of the vertical scanning of the drum obtained using the MCNP6 model with the experimental data acquired at the SAPHIR platform.

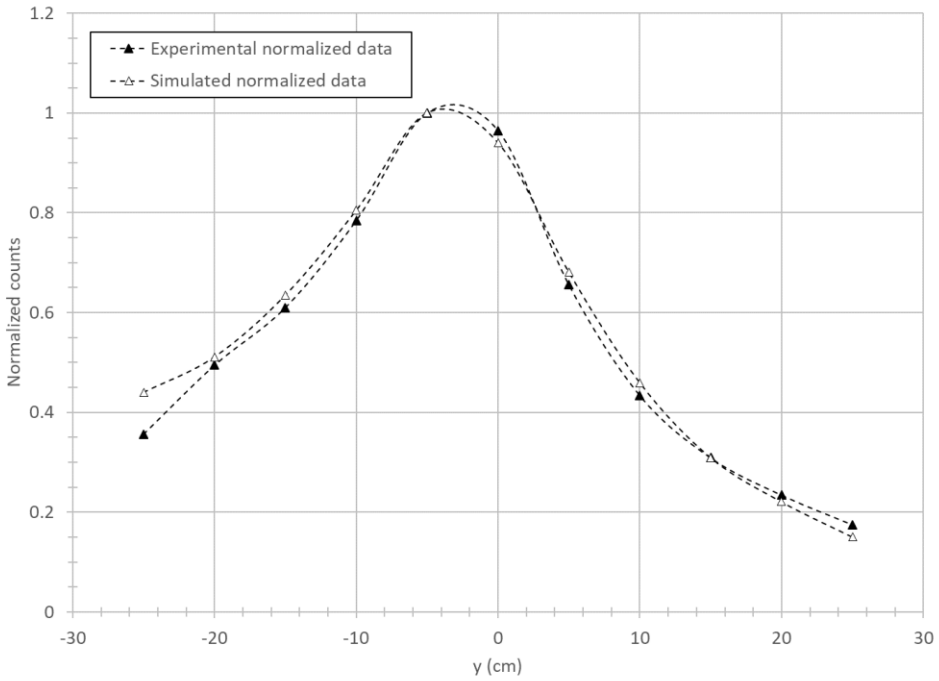

Figure 16. Comparison of the horizontal scanning of the drum obtained using the MCNP6 model with the experimental data acquired at the SAPHIR platform.

Results presented in Figs. (15)-(16) indicate that there is an agreement in the shape of the obtained counting curves. The MCNP6 model presents a satisfactory behavior and is further used in the next section of the article for assessment of virtual cases.

3.7. Assessment of virtual cases by Monte-Carlo simulation

The goal of this Monte Carlo study was to gain knowledge on the photofission rates and detection efficiencies with other matrix materials at 7 and 9 MeV interrogation energies using the validated numerical model of the measurement setup described above. Configurations that could not be tested at the SAPHIR platform could be assessed thanks to the MCNP6 simulation model previously validated.

Three virtual cases imply a homogeneous matrix, which fills the entire 220-L drum volume. Three different matrix materials were selected: (1) concrete matrix (ρ=2.4 g/cm^3); (2) PVC plastic matrix (ρ=0.3 g/cm^3) and (3) steel matrix (ρ=3.9 g/cm^3). Compositions of PVC and steel matrices are displayed in Tables (8) and (9) respectively. Composition of concrete was given in Table (1). A 3D representation of a virtual case with concrete matrix is shown in Fig. (17).

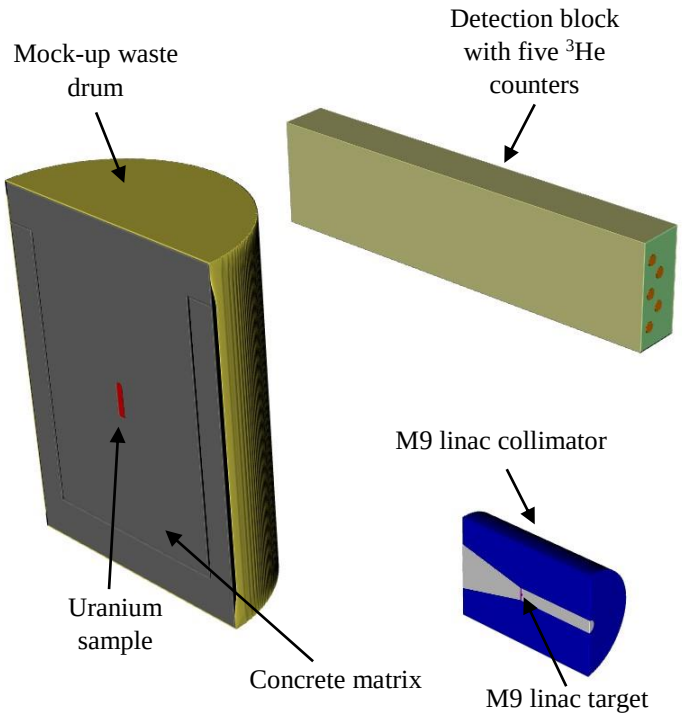

Fig. 17. Virtual concrete filled mock-up drum case.

Table 8. PVC matrix composition.

Element	Weight fraction, %
H	4.8382
C	38.4361
Cl	56.7257

Table 9. Steel matrix composition.

Element	Weight fraction, %
C	0.15000
Mn	0.30000
^{28}Si	0.23055
^{29}Si	0.01170
^{30}Si	0.007725
^{54}Fe	5.804085
^{56}Fe	91.07796
^{57}Fe	2.184600
^{58}Fe	0.278040

The determined photofission rates and detection efficiencies are summarized in Table (10). For these calculations, linac operating frequency of 100 Hz was used. As a reminder, the electron peak current was 100 mA and the pulse duration was 2.5 μs.

Table 10. Summary of results obtained with the virtual cases studied at 7 or 9 MeV.

Parameter	Virtual case		
	Concrete matrix	PVC matrix	Steel matrix
Hydrogen component, %	0.75	50	0
Detection efficiency, %	0.0470	0.0167	0.3030
Photofission rate, fission/s at 7 MeV	4.83E+05	1.40E+06	1.07E+05
Photofission rate, fission/s at 9 MeV	7.47E+06	2.01E+07	1.60E+06

As expected, results indicate that the detection efficiency for virtual cases with concrete and PVC matrices is lower by a factor of fifteen than that with a reference mock-up drum case presented in Table (3). For a virtual case with a concrete matrix, such a behavior is dictated by attenuation of the neutron response in homogeneous matrix that fills the entire volume of the drum. For a virtual case with a PVC matrix, such a behavior is due to moderation of the neutron response below the cadmium material threshold covering the detection block. As for the case with a steel matrix, the detection efficiency is slightly higher than that of a reference mock-up drum case due to low attenuating properties of steel for neutrons. The determined detection efficiencies confirm that there is an impact of the presence of the hydrogen component in the matrix materials. Thus, for a concrete matrix it leads to a value lower by a factor 5.3 and for a PVC matrix by a factor 15 compared to the reference case (ε=0.250%), presented in Tables (6) and (7) at y=0, z=0. The detection efficiency for the case with a steel matrix is not better than that of reference mock-up drum due to higher density (ρ=3.9 g/cm^3 for steel matrix vs ρ=2.4 g/cm^3 for concrete).

The determined photofission rates for virtual cases show that in the case of a steel matrix filling the entire volume of the drum the photofission rate is lower for both 7 and 9 MeV electron energies compared to the reference mock-up drum case used during the measurement campaign conducted at the SAPHIR platform. This is due to a strong attenuation of the incident *Bremsstrahlung* beam of photons in such a matrix. However, with a PVC matrix the observed photofission rate is the highest among all studied cases due to the very little effect of such a matrix on the incident beam of photons. The photofission rate obtained with a concrete matrix covering the entire interior of the drum falls in the middle of all three studied virtual cases due to its attenuating effect on the incident beam of photons.

Nevertheless, these first results of the photofission technique performed at 7 MeV endpoint energy show the potential of this technique to characterize 220-L nuclear waste drums with a variety of different matrix materials.

4. Conclusion and outlook

In this paper, a performance assessment of the photofission technique for the radiological characterization of 220-L nuclear waste drums with homogeneous, dense and voluminous matrices using 7 or 9 MeV linacs was presented. Reference measurements at 9 MeV were conducted at the SAPHIR platform (CEA Paris-Saclay) using a 9 MeV linac and a mock-up drum with a 6.5 cm-thick concrete liner, and showed that 0.336 grams of 94% ^{239}Pu and 0.539 grams of depleted uranium can be detected in 10 min with one detection block comprised of five ^{3}He tubes (150NH100). We also showed that potential hotspots could be localized by carrying out vertical and horizontal scanning of the drum. Such a characterization showed an equal sensitivity in both directions, indicating a 6-times difference in the counting statistics between the extreme and center positions. Then, an MCNP6 model of the measurement setup was developed and validated relatively to the experimental data. This simulation model was used to evaluate the performances of the photofission technique achieved with drums composed of other homogeneous matrices (concrete, PVC and steel) that fill the entire volume of the drum. The model was also used to extend the study to the use of a 7 MeV endpoint energy (close to the energy threshold of the photofission reaction, which is around 6 MeV for most actinides). Our results confirm that the efficiency for total delayed neutron counting is a function of the hydrogen component presence in the matrix. Thus, for PVC plastic and concrete matrices that fill the entire volume of a 220-L drum it is lower than that for a reference case (6.5 cm-thick concrete liner) by factors 5.3 and 15 respectively. The detection efficiency for the case with a steel matrix is worse than that for a reference mock-up drum case by a factor of 1.2 due to its higher density. Another important aspect is related to the production of parasitic photoneutrons due to (γ, n) reactions in the target, collimator and surrounding materials. With our results, we find that at both 7 and 9 MeV endpoint energies they are present and that the relative portion of fissions caused by photoneutrons is 3.9 % and 4.4 % respectively for a reference mock-up drum case and a depleted uranium sample. However, the photofission rate at 7 MeV is 15-times lower for all studied cases, compared to 9 MeV.

The first reference measurements coupled with Monte Carlo modeling and study of different virtual cases demonstrated the potential of the photofission technique for characterization of 220-L nuclear waste drums with a variety of different homogeneous matrix materials using linacs operated at 7 and 9 MeV endpoint energies. Another important aspect is related to lower dose-burden of a linac system operated at 7 MeV what coupled with the compact design of such

systems opens new horizons for their application on mobile platforms aiming at *in-situ* radiological characterization of nuclear waste packages. Performance assessment of the photofission technique applied to characterization of nuclear waste packages with heterogeneous matrix materials is an interesting premise for future research in this domain.

5. Funding

This project has received funding from the European Union's Horizon 2020 research and innovation programme under grant agreement No 847641. The work presented in this paper reflects only the author's views and the Commission is not liable for any use that may be made of the information contained therein.

6. Acknowledgements

The team would like to thank Hamid Makil for his assistance during the measurement campaign with mock-up drums at the SAPHIR platform housed at CEA Paris-Saclay.

7. References

[1] European Union H2020 Micado project website https://www.micado-project.eu/;

[2] Lyoussi A., Romeyer-Dherbey J., Jallu F., Payan E., Buisson A., Nurdin G., Allano J., "Transuranic waste detection by photon interrogation and on-line delayed neutron counting," Nucl. Instrum. Methods Phys. Res. B, vol. 160, (2000) pp. 280-289, (Pubitemid 30531389);

[3] Gmar M., Jeanneau F., Laine F., Makil H., Poumarede B., Tola F., "Assessment of actinide mass embedded in large concrete packages by photon interrogation and photofission," Appl. Radiat. Isot., vol. 63, (2005) pp. 613–619;

[4] Carrel F., Agelou M., Gmar M., Lainé F., Loridon J., Ma J.-L., Passard C., Poumarède B., "Identification and Differentiation of Actinides Inside Nuclear Waste Packages by Measurement of Delayed Gammas," in IEEE Transactions on Nuclear Science, vol. 57, no. 5, pp. 2862-2871, Oct. 2010, doi: 10.1109/TNS.2010.2064334;

[5] Kavouras J., Wen X., Norman D. R., Nakazawa D. R., Yang H., "Pulsed photofission delayed gamma ray detection for nuclear material identification," 2012 IEEE Nuclear Science Symposium and Medical Imaging Conference Record (NSS/MIC), 2012, pp. 95-100, doi: 10.1109/NSSMIC.2012.6551068;

[6] Sari A., Carrel F., Laine F., Lyoussi A., "Neutron interrogation of actinides with a 17 MeV electron accelerator and first results from photon and neutron interrogation non-simultaneous measurements combination," Nucl. Instrum. Methods Phys. Res. B, vol. 312, (2013) pp.30-35. (10.1016/j.nimb.2013.06.020);

[7] Simon E., Jallu F., Pérot B., Plumeri S., "Feasibility study of fissile mass quantification by photofission delayed gamma rays in radioactive waste packages using MCNPX," Nuclear Instruments and Methods in Physics Research Section A: Accelerators, Spectrometers, Detectors and Associated Equipment, ISSN: 0168-9002, Vol: 840, Page: 28-35, 2016;

[8] Sari A., Carrel F., Lainé F., "Characterization and Optimization of the Photoneutron Flux Emitted by a 6- or 9-MeV Electron Accelerator for Neutron Interrogation Measurements," in IEEE Transactions on Nuclear Science, vol. 65, no. 9, pp. 2539-2546, Sept. 2018, doi: 10.1109/TNS.2018.2857919;

[9] Dighe P. M., Vinod M., Thombare S. G., Prafulla S., Kamble N. R., Kamble L. P., Bhatnagar P. V., Das D., "Photofission Method for Quantification of Fissile Material in Large Drums," Nuclear Instruments and Methods in Physics Research, Section A: Accelerators, Spectrometers, Detectors and Associated Equipment, ISSN: 0168-9002, Vol: 946, Page: 162624, 2019;

[10] Meleshenkovskii I., Ogawa T., Sari A., Carrel F., Boudergui K., "Optimization of a 9 MeV Electron Accelerator Bremsstrahlung Flux for Photofission-based Assay Techniques Using PHITS and MCNP6 Monte Carlo Codes," Nuclear Instruments and Methods section B, Volume 483, (2020) 5-14;

[11] Morel J., Bickel M., Hill C., Verbruggen A., "Results of the international Pu-2000 exercise for plutonium isotopic composition measurements," Appl. Radiat. Isot. 60 (2004) 607;

[12] http://www.nucleide.org/Spectra_WG/Documentation/U-Pu-Library.pdf (sample E);

[13] Werner C. J., Bull J. S., Solomon C. J., Brown F. B., McKinney G. W., Rising M. E., Dixon D. A., Martz R. L., Hughes H. G., Cox L. J., Zukaitis A. J., Armstrong J. C., Forster R. A., Casswell L., "MCNP6.2 Release Notes", LA-UR-18-20808 (2018);

[14] Sibczynski P., Dziedzic A., Grodzicki K., Iwanowska J., Kosinski T., Matusiak M., Moszynski M., Swiderski L., Syntfeld-Kazuch A., Wolski D., Frederick Carrel, Grabowski A., Hamel M., Laine F., Sari A., Iovene A., Tintori C., "Comparison of prompt and delayed photofission neutron detection techniques using different types of radiation detectors," 2016 IEEE Nuclear Science Symposium, Medical Imaging Conference and Room-Temperature Semiconductor Detector Workshop (NSS/MIC/RTSD), Strasbourg, (2016) 1-3;

[15] Dighe P. M., Berthoumieux E., Doré D., Laborie J. M., Ledoux X., Macary V., Panebianco S., Ridikas D., Laborie J. M., Ledoux X., "Delayed gamma studies from photo-fission of 237Np for nuclear waste characterization," Annals of Nuclear Energy, 36 (3), 399–403, 2009;

[16] Carrel F., Agelou M., Gmar M., Lainé F., "Detection of high-energy delayed gammas for nuclear waste packages characterization," Nuclear Instruments and Methods in Physics Research Section A: Accelerators, Spectrometers, Detectors and Associated Equipment, ISSN: 0168-9002, Volume 652, Issue 1, (2011) 137-139.

[17] Delarue M., Simon E., Pérot B., Allinei P. G., Estre N., Payan E., Eck D., Tisseur D., Espagnon I., Collot J., "Measurement of cumulative photofission yields of 235U and 238U with a 16 MeV Bremsstrahlung photon beam," Nuclear Instruments and Methods in Physics Research, Section A: Accelerators, Spectrometers, Detectors and Associated Equipment, 1011, 2021;

[18] Foley A., Yang H., "Short-lived photofission product yields from 238U and 232Th at Bremsstrahlung X-ray endpoint energies of 8, 14, and 20 MeV for nuclear forensics isotope production applications," Nuclear Instruments and Methods in Physics Research, Section A: Accelerators, Spectrometers, Detectors and Associated Equipment, 1013, 2021.

[19] Finch S. W., Bhike M., Howell C. R., Krishichayan, Tornow W., Tonchev A. P., Wilhelmy J. B., "Measurements of Short-Lived Isomers from Photofission as a Method of Active Interrogation for Special Nuclear Materials," Phys. Rev. Applied, Vol. 15, Iss. 3, 2021;

[20] De Stefano R., Carasco C., Pérot B., Simon E., Nicol T., Mauerhofer E., "Feasibility study of fissile mass detection in 870 L radioactive waste drums using delayed gamma rays from

neutron-induced fission," Journal of Radioanalytical and Nuclear Chemistry, (2019) 1185–1194 https://doi.org/10.1007/s10967-019-06731-2.